

Endoplasmic Reticulum Stress Implicated in the Development of Renal Fibrosis

Chih-Kang Chiang,^{1,2} Shih-Ping Hsu,^{2,3} Cheng-Tien Wu,⁴ Jenq-Wen Huang,² Hui-Teng Cheng,² Yi-Wen Chang,^{1,2} Kuan-Yu Hung,² Kuan-Dun Wu,² and Shing-Hwa Liu⁴

¹Department of Integrated Diagnostics and Therapeutics, National Taiwan University Hospital and National Taiwan University College of Medicine, Taipei, Taiwan; ²Department of Internal Medicine, National Taiwan University Hospital and National Taiwan University College of Medicine, Taipei, Taiwan; ³Division of Nephrology, Far Eastern Memorial Hospital, Taipei, Taiwan; and ⁴Institute of Toxicology, School of Medicine, National Taiwan University, Taipei, Taiwan

Endoplasmic reticulum (ER) stress-associated apoptosis plays a role in organ remodeling after insult. The effect of ER stress on renal tubular damage and fibrosis remains controversial. This study aims to investigate whether ER stress is involved in tubular destruction and interstitial fibrosis *in vivo*. Renal cell apoptosis was proven by terminal deoxynucleotidyl transferase dUTP nick end-labeling (TUNEL) stain and poly-ADP ribose polymerase expression in the unilateral ureteral obstruction (UUO) kidney. ER stress was evoked and confirmed by the upregulation of glucose-regulated protein 78 (GRP78) and the common Lys-Asp-Glu-Leu (KDEL) motif of ER retention proteins after UUO. ER stress-associated proapoptotic signals, including B-cell chronic lymphocytic leukemia (CLL)/lymphoma 2-associated x protein (BAX) expression, caspase-12 and c-Jun N-terminal kinase (JNK) phosphorylation, were activated in the UUO kidney. Prolonged ER stress attenuated both unsplicing and splicing X-box binding protein 1 (XBP-1) protein expression, but continued to activate inositol-requiring 1 α (IRE1 α)-JNK phosphorylation, protein kinase RNA-like endoplasmic reticulum kinase (PERK), eukaryotic translation initiation factor 2 α subunit (eIF2 α), activating transcription factor (ATF)-4, CCAAT/enhancer binding protein (C/EBP) homologous protein (CHOP) and cleavage activating transcription factor 6 (cATF6)-CHOP signals, which induce ER stress-related apoptosis but attenuate adaptive unfolded protein responses in UUO kidneys. However, renal apoptosis and fibrosis were attenuated in candesartan-treated UUO kidney. Candesartan was associated with maintenance of XBP-1 expression and attenuated ATF4, cATF6 and CHOP protein expression. Taken together, results show that overwhelming ER stress leads to renal cell apoptosis and subsequent fibrosis; and candesartan, at least in part, restores renal integrity by blocking ER stress-related apoptosis. Reducing ER stress may present a way to attenuate renal fibrosis.

© 2011 The Feinstein Institute for Medical Research, www.feinsteininstitute.org

Online address: <http://www.molmed.org>

doi: 10.2119/molmed.2011.00131

INTRODUCTION

Renal fibrosis, considered the common consequence of progressive renal disease, involves glomerulosclerosis and/or tubulointerstitial fibrosis (1,2). Much interest has focused on investigating potential mechanisms to prevent or reverse the damage (3). A number of stressors, including ischemia, hypoxia and oxidative injury, contribute to renal cell loss as renal

fibrosis progresses (1,2,4,5). Apoptosis, a regulated energy-dependent cell death, is reported critical in renal cell loss and subsequent renal fibrosis (6,7). However, the detailed cellular mechanisms of tubular atrophy are still not fully understood, and appropriate approaches to minimize the risks are still being explored.

The endoplasmic reticulum (ER) is involved in the folding of secretory and

membrane proteins and in the apoptosis pathway (8). Renal cells have a well-developed ER, reflecting their role in filtering much cytokines and various glycoproteins. Many conditions disturb the ER function and result in ER stress, including ischemia, hypoxia, glucose starvation, elevated protein synthesis, gene mutation and failure in protein folding, transport or degradation (9–11). ER stress initiates three major signaling pathways, called the unfolded protein response (UPR) (12). Three sensors along the ER stress pathway are activating transcription factor (ATF)-6, inositol-requiring 1 α (IRE1 α) and protein kinase RNA-like endoplasmic reticulum kinase (PERK) (8). Unstressed, the three sensors are linked with the ER chaperone, glucose-regulated protein 78 (GRP78), but these UPR initiators are released from

Address correspondence and reprint requests to Kuan-Yu Hung, Department of Internal Medicine, National Taiwan University Hospital and National Taiwan University College of Medicine. Phone: +886-2-23123456, ext. 63288; Fax: +886-2-23222955; E-mail: kyhung@ntu.edu.tw; and Shing-Hwa Liu, Institute of Toxicology, College of Medicine, National Taiwan University, Taipei, 10051, Taiwan. Phone: +886-2-23123456 ext 88605.

Fax: +886-2-23410217; E-mail: shinghwaliu@ntu.edu.tw.

Submitted April 9, 2011; Accepted for publication August 18, 2011; Epub

(www.molmed.org) ahead of print August 19, 2011.

GRP78 when they encounter accumulated misfolded proteins in the ER, or depletion of ER calcium stores (8). When ATF6 is released from GRP78, it moves to the Golgi apparatus and then is cleaved by site-1 and site-2 proteases (13,14). The cleavage activating transcription factor 6 (cATF6) fragment has a DNA-binding domain with a basic leucine zipper motif and a transcriptional activation domain, which migrates to the nucleus to activate transcription of ER chaperones and enzymes, promoting protein folding, maturation and secretion to induce ER-associated degradation and CCAAT/enhancer binding protein (C/EBP) homologous protein (CHOP) expression (15). In parallel with ATF6, IRE1 α autophosphorylates and activates its endoribonuclease activity, forming splicing X-box-binding protein-1 (XBP-1) mRNA, which yields a potent transcriptional activator. Splicing XBP-1 protein in parallel with ATF6 activates transcription of the ER-associated degradation and oxidant detoxifying enzymes (8,16,17). The third part of the ER stress response involves PERK, which is activated through homodimerization and transphosphorylation, allowing PERK to phosphorylate the eukaryotic translation initiation factor-2 α subunit (eIF2 α). In turn, the recognition of the AUG codon is reduced, and the general translation is turned down to decrease the ER protein load (18). Meanwhile, ATF4 can be preferentially translated and induce expression of UPR target genes. Differential expression of ER stress proteins may lead to cell survival or apoptosis, which may, in turn, guide the prognosis of renal disease involved in ER stress (18,19).

Recently, ER stress has been shown in the development of heart and liver fibrosis (20–22). Using proteomics, Dihazi *et al.* (23) elegantly demonstrated that ER stress-related proteins were highly up-regulated in the renal fibroblast of fibrotic kidney. In this study, we applied the rat unilateral ureteral obstruction (UVO) model to study the implication of ER stress in renal fibrosis. UVO is associated with induction of hypoxia, oxidative stress and activation of the renin an-

Table 1. Blood pressure and renal function test of UVO- and CAN-treated rats.

	Sham	UVO	UVO/CAN	CAN
Systolic blood pressure (mmHg)	106 \pm 6	135 \pm 10 ^a	111 \pm 8	104 \pm 6
Diastolic blood pressure (mmHg)	84 \pm 5	98 \pm 8 ^a	88 \pm 6	82 \pm 5
Blood urea nitrogen (mg/dL)	18.2 \pm 0.8	35.8 \pm 2.9 ^a	24.8 \pm 1.9	18.8 \pm 0.8
Creatinine (mg/dL)	0.58 \pm 0.04	0.60 \pm 0.05	0.59 \pm 0.05	0.58 \pm 0.05

^aStatistically significant compared with sham operation: $P < 0.05$.

giotensin system during the development of renal fibrosis (24,25). Recently, Badiola *et al.* (26) suggested that oxygen-glucose deprivation or neonatal hypoxia-ischemia activates ER stress signals and leads to ER-dependent neuron cell death (26). Antioxidants also successfully suppressed epithelial-to-mesenchymal transition and ER stress in the albumin-overloaded renal tubular cells (27). We believe that all hypoxia, metabolic distress and oxidative stress might contribute to UVO-induced ER stress induction. Furthermore, Yeh *et al.* (28) also demonstrated that UVO evoked tubular apoptosis via oxidative and ER stress *in vivo*. These results support the assertion that activation of ER stress may contribute to tissue fibrosis, including renal fibrosis.

On the basis of these studies, we hypothesized that kidney of UVO suffers from hypoxia (24), which is known to induce ER stress (26) and then contribute to the tubular damage and renal fibrosis. To prove our hypothesis, we tried to demonstrate the sequential activation of ER stress by using the UVO fibrosis model and explore the time-dependent correlations between the activation of ER stress signals and renal cell apoptosis/interstitial fibrosis.

MATERIALS AND METHODS

Experimental Protocols

UVO surgery was introduced in male Wistar rats (150–200 g). Experimental animals were sacrificed at d 1, 3, 7 and 14 to analyze the differential activation of UPR proteins. Each time point included at least four independent experiments. Previous study showed candesartan (CAN) (Takeda Pharmaceuticals, Osaka, Japan), an angiotensin type II receptor blockade

(ARB), ameliorated interstitial fibrosis in association with suppression of heat-shock protein 47 expression in the UVO model (29). Heat-shock protein 47 was considered to be a collagen-specific molecular chaperone that plays a pivotal role during the biosynthesis and secretion of procollagen from ER (29). This study prompted us to choose CAN as a therapeutic intervention to ameliorate renal fibrosis and ER stress through modulating chaperon and homeostasis of ER. We have chosen the standard dose (5 mg/kg/day) using in a long-term, high-dosage CAN study in our experiment (30). Four groups of rats were arranged for therapeutic intervention experiments. UVO rats were treated with either vehicle (UVO group, $n = 4$) or CAN (5 mg/kg/day; UVO/CAN group, $n = 4$) by oral gavages from d 0 to 13. Sham operation (sham and sham/CAN group) was performed in six age-matched rats. At d 14, a multiple physiological recorder (TA240S; Gould, Valley View, OH, USA) was applied to record arterial blood pressure and heart-beat rate through the carotid artery and then the blood was sampled and rats were sacrificed. The information of blood pressure and biochemical parameters were shown in Table 1. Kidney tissues were fixed in 10% neutral-buffered formalin solution and paraffin-embedded for Periodic acid-Schiff and immunohistochemical staining. Tissues were frozen to -70°C and stored for later immunofluorescence staining and protein extraction. All animal experiments were performed in accordance with the National Institutes of Health guidelines for use and care of laboratory animals and approved by the review boards of the Experimental Animal Center, College of Medicine, National Taiwan University, Taipei, Taiwan.

Table 2. Antibodies used for immunohistochemistry and immunofluorescence and Western blot.

Primary antibody	Company	Catalog number
ATF4	Abcam, Cambridge, MA, USA	ab50546
ATF6	Imgenex Corporation, San Diego, CA, USA	IMG-273
Bax	GeneTex, Alton Parkway, Irvine, CA, USA	GTX61026
Caspase12	AB cam (Abcam)	ab18766
CHOP	Santa Cruz Biotechnology, Santa Cruz, CA, USA	sc 7351
Collagen type 1	Abcam	ab6308
eIF2 α	Santa Cruz Biotechnology	sc133132
p-eIF2 α	Cell Signaling Technology, Danvers, MA, USA	119A11, #3597
Fibronectin	GeneTex	GTX61206
GAPDH	Santa Cruz Biotechnology	sc-717379
GRP78	Santa Cruz Biotechnology	sc-13968
IRE1 α	Cell Signaling Technology	#3183
p-IRE-1 (ser 724)	Novus Biologicals, Littleton, CO, USA	NB1002323
p-JNK	Santa Cruz Biotechnology	sc-7106
KDEL	AB cam (Abcam)	ab69659
PARP	Cell Signaling Technology	#9542
PERK	Santa Cruz Biotechnology	sc-13073
p-PERK	Santa Cruz Biotechnology	sc-32577
α -SMA	Sigma Chemical, St. Louis, MO, USA	a2547
XBP-1	Santa Cruz Biotechnology	sc-7106

Electrophoresis and Immunoblotting

Whole kidney tissue lysates were prepared as described previously. Proteins were separated by precast 10% sodium dodecyl sulfate–polyacrylamide gel electrophoresis and then electrophoretically transferred from the gel onto polyvinylidene difluoride membranes. After blocking, blots were incubated with primary antibodies (Table 2) in phosphate-buffered saline (PBS) with 0.1% Tween 20 followed by three 10-min washes in PBS with 0.1% Tween 20. The membranes were then incubated with horseradish peroxidase–conjugated secondary antibodies for 60 min. Western blotting reagent ECL (Amersham, Little Chalfont, UK) was used to detect protein expression, and Kodak X-Omat film (Kodak, Rochester, NY, USA) was used to show chemiluminescence. Evaluation of Western blot bands was performed by densitometric analysis using NIH Image J 1.310 software.

Semiquantitative Assessment of Renal Fibrosis

Tubulointerstitial fibrosis was graded by degree of interstitial collagen deposition using Masson trichrome–stained sections (0 = no staining; 1 = <25% staining;

2 = 25% to 50% staining; 3 = 50% to <75% staining; 4 = 75% to 100% staining of the section) (31). Tubulointerstitial damage was scored for each rat and averaged by group. The same investigator, blinded to the nature of the experiment, analyzed all renal pathology samples.

Immunohistochemical Analysis

Sections of 6 μ m were stained using the indirect immunoperoxidase method. The first antibody used was anti-KDEL Polyclonal Antibody (Abcam, Cambridge, MA, USA). Briefly, 6- μ m renal sections were microwaved (model TMO-6810; Tatung, Taipei, Taiwan) in 0.01 mmol/L citrate buffer, pH 6.0, for 2–5 min at 800 W to retrieve the antigens. The sections were then treated with 0.5% hydrogen peroxide in 1 \times PBS for 20 min at room temperature to block the endogenous peroxidase. Sections were subsequently blocked with 10% normal goat serum for 30 min at room temperature, and primary antibodies were then added, followed by incubation at 4°C overnight. The next day, sections were washed three times in 1 \times PBS/0.1% Triton X-100 for 10 min and incubated in biotin-conjugated anti-rabbit immunoglobulin G for 1 h at room tem-

perature. The sections were then incubated with the avidin-biotin-peroxidase reagent for another 1 h at room temperature according to the manufacturer's instructions (Dako, Glostrup, Denmark). Reactions on sections were detected with peroxidase substrate containing diaminobenzidine chromogen enhanced with 1.5% ammonium nickel sulfate (for KDEL staining). For negative controls, the specific antibodies were omitted.

Immunofluorescence Analysis

For apoptosis assay, 6- μ m frozen sections were stained with terminal transferase-mediated dUTP nick end-labeling reagent (Promega, Madison, WI, USA) and 4',6-diamidino-2'-phenylindole dihydrochloride for *in situ* apoptosis detection. In brief, 6- μ m frozen sections were treated with 20 μ g/mL proteinase K and then incubated in a nucleotide mixture containing fluorescein-12-dUTP and terminal deoxynucleotidyl transferase. Positive controls were pretreated with 1 U/mL DNase, and negative controls were incubated without terminal deoxynucleotidyl transferase. To evaluate CHOP expression, anti-CHOP monoclonal antibody (Santa Cruz Biotechnology, Santa Cruz, CA, USA) was used. Samples were labeled with fluorescent-conjugated affinity purified secondary antibody, colabeled with 4',6-diamidino-2'-phenylindole (DAPI) and mounted with Vectashield (VectorLabs, Burlingame, CA, USA). Twenty high-power fields (200 \times) were randomly selected, and the value of fluorescent apoptotic cells was counted. The mean of apoptotic cells per high-power field was expressed.

Statistical Analysis

The values given here are presented as mean \pm standard error of the mean (SEM). All analyses were performed using Student *t* test. *P* < 0.05 was considered statistically significant. All statistical calculations were performed with SPSS 16.0 for Windows (SPSS, Chicago, IL, USA).

All supplementary materials are available online at www.molmed.org.

RESULTS

Tubular Cells Apoptosis and Renal Fibrosis Developed in the Rat UUO Model

Poly-ADP ribose polymerase (PARP), which regulates the nuclear machinery used to repair damaged DNA, was 4.7 times more upregulated 24 h after UUO, and upregulation continued up to 10.0 times induction until the end of observation (Figure 1A). After UUO, tubular cell apoptosis, as demonstrated by terminal deoxynucleotidyl transferase dUTP nick end-labeling (TUNEL) staining, was increased since d 1 and significantly enhanced at d 14 (Figures 1D–H). The development of renal fibrosis in the UUO kidney was shown in Figure 2. At d 3 after UUO (Figure 2B), Masson trichrome staining showed tubular dilation and increased interstitial volume, but showed no significant interstitial fibrosis over sham-operative kidney (Figure 2A). Tubular dilation and interstitial volume increased, whereas fibrosis developed progressively on d 7 (Figure 2C) and d 14 (Figure 2D) after UUO. Renal fibrosis increased over time, as shown by interstitial collagen deposition score (Figure 2E). These findings confirm that our models produced tubular apoptosis and progressive renal fibrosis.

Induction of ER Chaperone and Retention Proteins in UUO Kidney

GRP78, a molecular chaperone of ER, is used extensively to indicate the induction of ER stress. As shown in Figure 3A, Western blot analysis showed that basal levels of GRP78 were expressed in the renal tissue of control kidney. UUO enhanced GRP78 chaperone 2.3 times by d 1, and this elevation persisted but was slightly attenuated (2.0 times that of sham operation) until the end of observation at d 14. The carboxy-terminal amino acid sequence KDEL (Lys-Asp-Glu-Leu) is a common motif of ER permanent retention proteins (32). At d 3 after UUO (Figure 3C), immunohistochemical staining showed that the expression of KDEL-positive proteins was

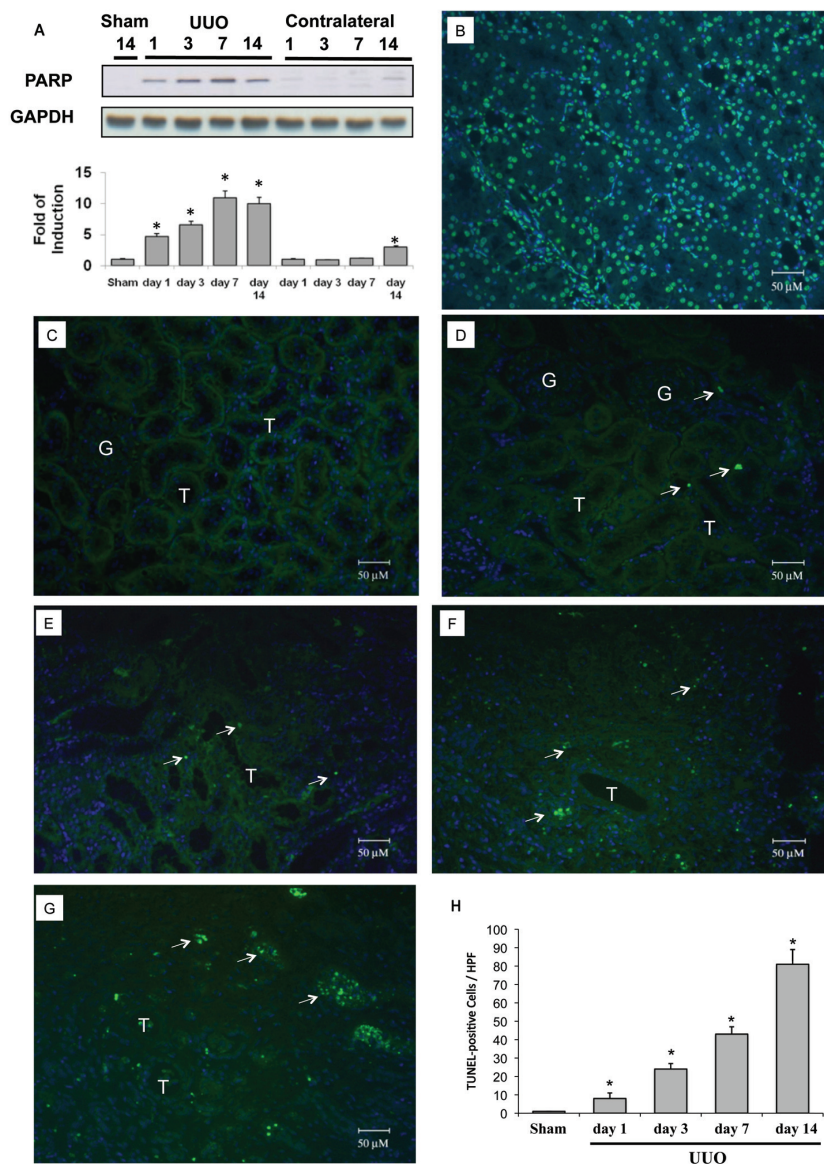


Figure 1. Cleaved PARP and apoptosis in rat kidneys subjected to UUO. The left kidneys of male Wistar rats were subjected to UUO as described in Materials and Methods. Kidneys were harvested 1, 3, 7 or 14 d after UUO. (A) Cleaved PARP expression in the whole kidney lysate was evaluated via Western blot analysis using antibodies against these proteins, with GAPDH used as a loading marker. PARP was 4.7 times more upregulated 1 d after UUO and up to 10.0 times more upregulated on days 7–14. Protein bands were quantified and presented as mean \pm standard error of the mean (SEM) for each group ($n = 4$). $*P < 0.05$ versus sham operation (Sham) group. Apoptosis was evaluated via a TUNEL assay. (B) DNAase-treated kidney section was used as a positive control for TUNEL staining. (C) Sham-operative kidneys show no positive nuclear stain for TUNEL. (D–G) UUO kidney showed a significant increase in TUNEL-positive staining at day 1, 3, 7 or 14. (H) The TUNEL-positive staining cells of the kidney tissue graded quantitatively as described in Materials and Methods were averaged for rats of each group ($n = 4$). $*P < 0.05$ versus the sham operation (Sham) group. The arrows indicate TUNEL-positive cells. G indicates glomerulus and T is renal tubule. 4',6-Diamidino-2-phenylindole (DAPI) staining was used to stain the nuclei blue. HPF, high power field.

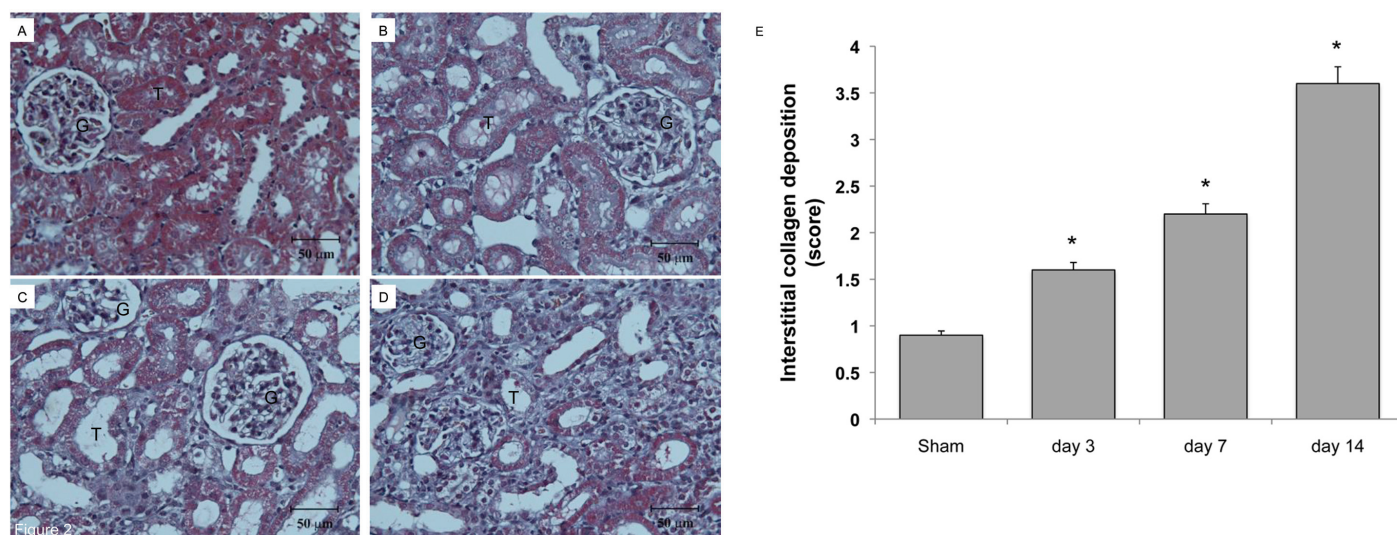


Figure 2. Collagen deposition in rat kidneys subjected to UUO. The left kidneys of male Wistar rats were subjected to UUO as described in Materials and Methods. At 3, 7 and 14 d after UUO, the kidneys were harvested and cut into 6- μ m-thick slices for Masson trichrome staining. (A) Sham-operative kidneys showed no positive Masson trichrome staining. (B) Three days after UUO, slight tubular dilation and interstitial volume expansion was observed. Persistent ureteral obstruction induced progressive tubular dilation, interstitial volume expansion and development of fibrosis at day 7 (C) and day 14 (D) after UUO. (E) The degree of interstitial collagen deposits in Masson trichrome-stained sections of the kidney tissue graded semiquantitatively as described in Materials and Methods was averaged for rats of each group ($n = 4$ for each group). * $P < 0.05$ versus the sham operation (Sham) group.

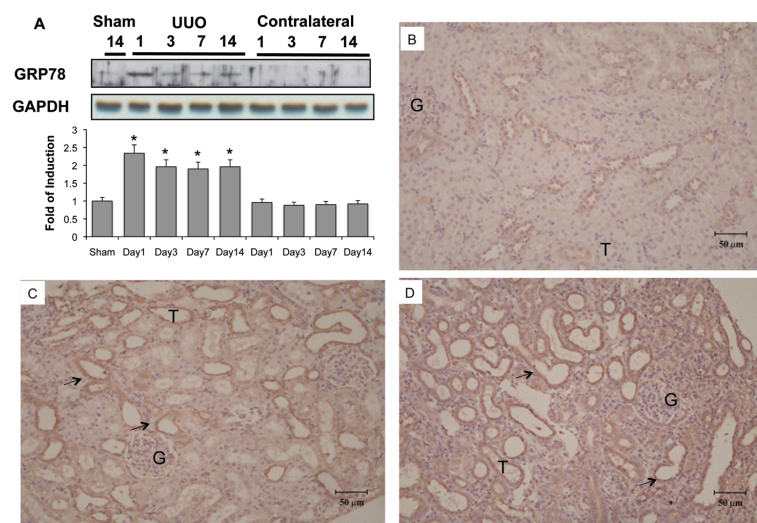


Figure 3. Induction of ER chaperone and ER retention proteins in kidneys subjected to UUO. Kidneys were harvested at 1, 3, 7 or 14 d after UUO. (A) GRP78 expression in the whole kidney lysate was determined by Western blot analysis using antibodies against this protein, with GAPDH used as a loading marker. Protein bands were quantified using Image J analysis software. Values are mean \pm standard error of the mean (SEM) ($n = 4$). * $P < 0.05$ versus the sham group. As compared with the sham operative kidney (B), the expression of carboxy-terminal amino acid sequence KDEL (Lys-Asp-Glu-Leu)-positive proteins were increased on the third day after UUO (C), as shown by immunohistochemical staining. KDEL-positive stained cells (arrow) were dominantly observed in the dilated tubules (D) at day 14. G indicates glomerulus and T is renal tubule.

increased compared with the sham-operative kidney (Figure 3B). KDEL-positive stained cells were dominant throughout the dilated tubules at d 14 (Figure 3D). These findings clearly demonstrate the continued and persistent activation of ER stress in UUO kidneys.

Overwhelming ER Stress Caused ER-Related Apoptosis in UUO Kidney

As mentioned previously, renal tubular cell apoptosis was induced in the UUO kidney (see Figure 1). The common effectors of ER-related apoptosis were also activated in the UUO kidney, including B-cell chronic lymphocytic leukemia (CLL)/lymphoma 2-associated \times protein (BAX) and caspase-12 (Figures 4A, B), phosphorylation of c-Jun N-terminal kinase (JNK) (Figure 4C) and CHOP (Figures 4D–H). Taken together, these results support the assertion that induction of ER stress-related apoptosis contributes significantly to the development of renal fibrosis. Under this hypothesis, we explored the upstream signals involved in the activation of ER-related apoptosis. In the in-

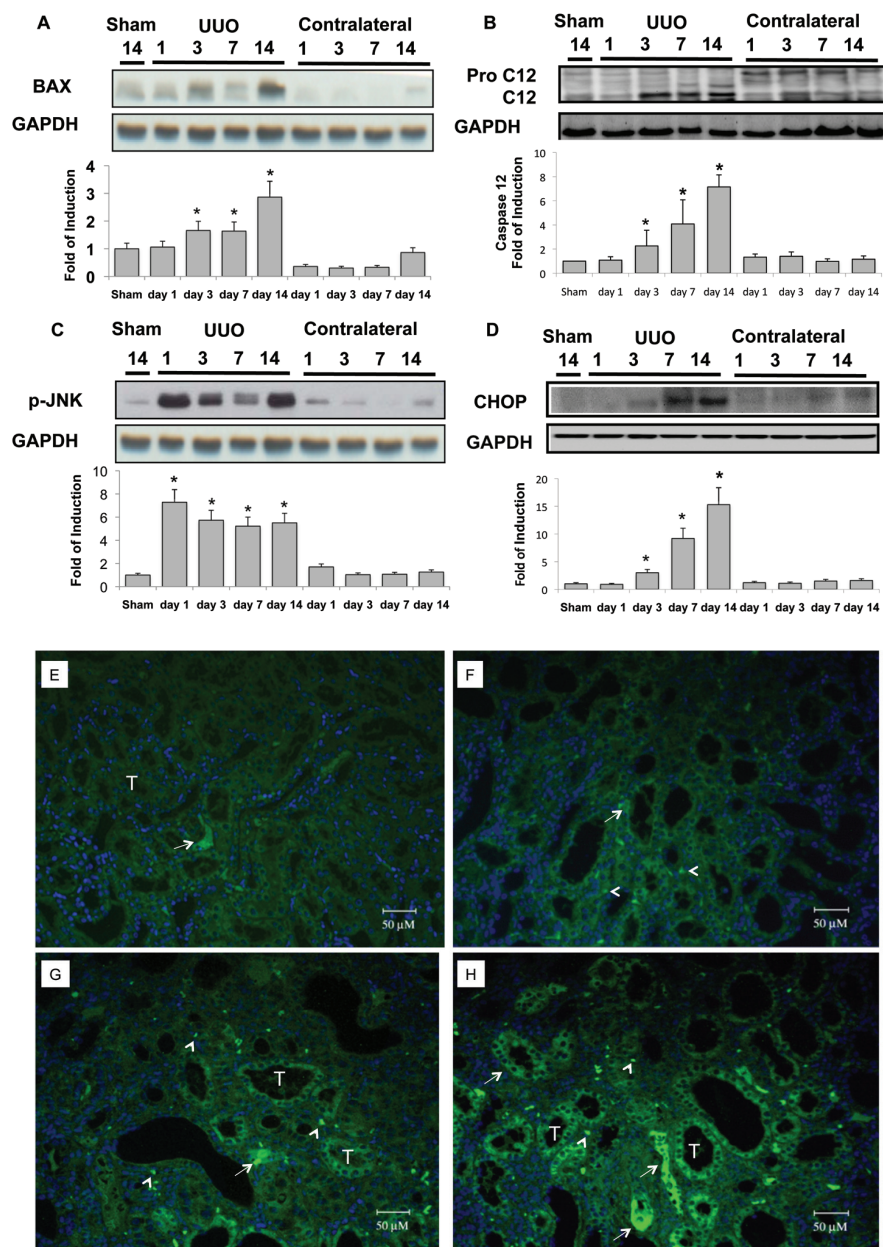


Figure 4. Activation of ER stress-related proapoptotic signals in the UUO kidney. UUO gradually enhanced BAX expression (A) and increased caspase-12 in the kidney in a time-dependent manner (B). At day 14, BAX expression was 2.9 times normal, and cleavage caspase-12 was 7.2 times that of basal levels in the UUO kidney. (C) Induction of phosphorylation of JNK (p-JNK) increased by 7.3 times at 24 h after UUO. This condition lasted until the end of observation at day 14, by which time it was 5.5 times basal level. (D) UUO induced 3.0, 9.2 and 15.3 times CHOP protein expression at days 3, 7 and 14, respectively. Protein bands were quantified and normalized by GAPDH using Image J analysis software. Values are mean \pm standard error of the mean (SEM) ($n = 4$). * $P < 0.05$ versus sham group. Immunofluorescence staining of CHOP was applied in the sham-operative kidneys (E) and UUO kidney at day 3 (F), day 7 (G) and day 14 (H). Progressive diffuse enhancement of CHOP fluorescence was shown in the tubular cytoplasm (arrow), and punctuated fluorescence dots localized at the nucleus (arrow head) in the UUO kidney. G indicates glomerulus and T is renal tubule.

active state, PERK, ATF6 and IRE1 α are linked by GRP78 on the ER membrane. PERK and eIF2 α phosphorylation activated at d 1 after UUO persisted throughout the observation period (Figures 5A, B). Downstream ATF4 signals were 10.7 times normal at d 1 after UUO, and this elevation also lasted until d 14, which implies the continued activation of PERK-eIF2 α phosphorylation-ATF4 signals in the UUO kidney (Figure 5C). Second, induction of ER stress resulted in ATF6 activation to the cATF6, which induced CHOP nuclear translocation and activated CHOP-dependent apoptosis. The cATF6 was detected after UUO and lasted until d 14 (Figure 5D). These findings are consistent with the induction of overwhelming ER stress and consequent renal tubular apoptosis (see Figure 1). Finally, on d 3 after UUO, overwhelming ER stress induced IRE1 α phosphorylation (Figure 5E), which enhanced the cleavage of procaspase-12 to caspase-12, JNK phosphorylation and ER-specific apoptosis (Figures 4B, C). On the other hand, IRE1 α phosphorylation is associated with XBP-1 splicing, which will lead to induction of ER-associated degradation and the ER chaperon, especially in the early stage of adaptive UPR. In the UUO model, at d 1 after ureteral obstruction, basal levels of unsplicing and splicing XBP-1 protein were suppressed, implying the diminishment of adaptive UPR (Figure 5F).

ARB Diminished Overwhelming ER Stress and Restored Adaptive UPR

CAN was administered on the d 1 after induction of rat kidney UUO. GRP78, a representative chaperon of ER stress, was induced 24 h after induction of UUO (see Figure 3). Early stage GRP78 expression implied the induction of adaptive UPRs, which are associated with the simultaneous maintenance of XBP-1 expression (Figure 5F). Fourteen days after UUO, the induction of ATF4, cATF6 and CHOP, as well as JNK phosphorylation, was consistent with PARP and caspase-12 (Figure 6). Treatment with CAN resulted in lower levels of cATF6, ATF4 and CHOP and less JNK

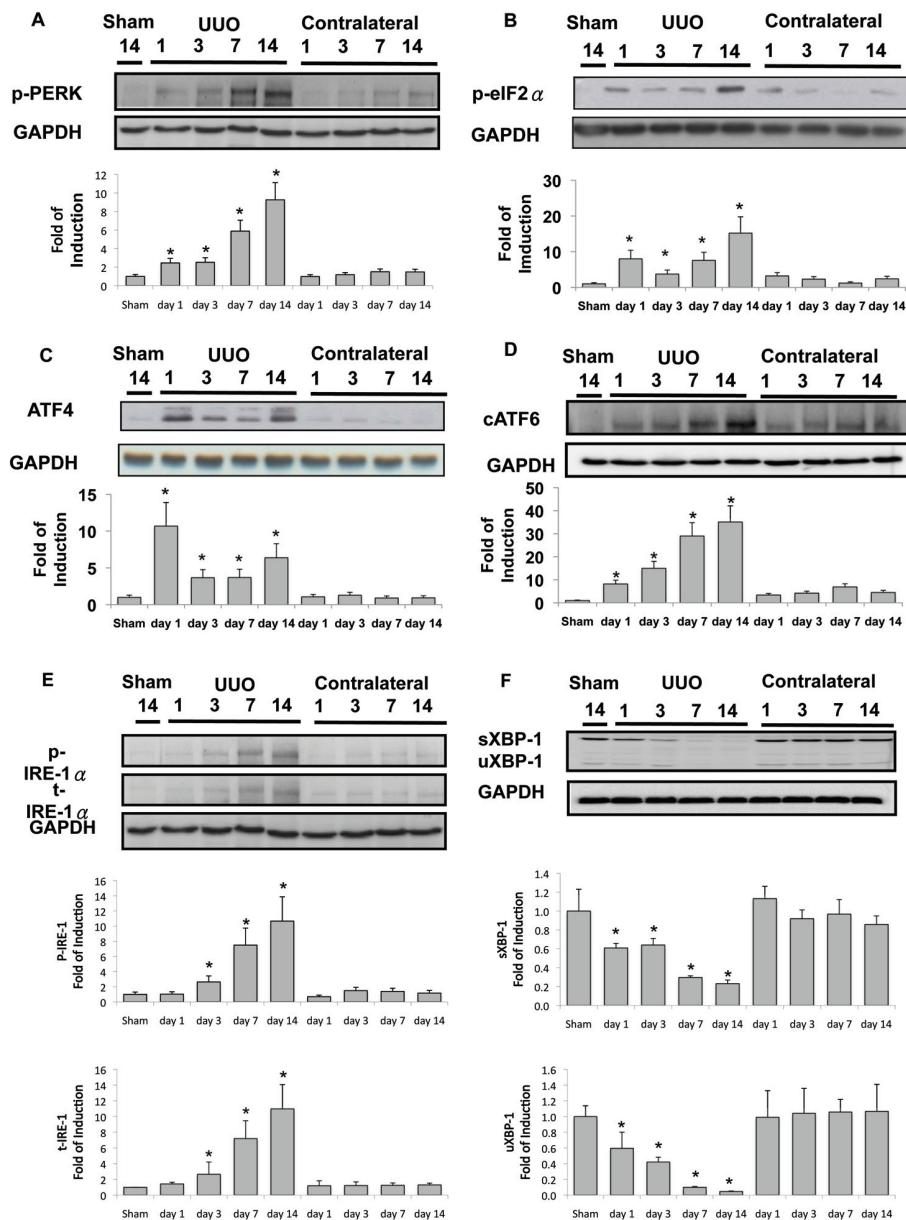


Figure 5. Diminished adaptive UPR and activation of overwhelming ER stress signals in the UUO kidney. (A) PERK phosphorylation was detected at basal conditions, and UUO gradually enhanced phosphorylation to 9.3 times the basal level at day 14. eIF2 α phosphorylation (B) and ATF4 protein expression (C) were induced abruptly after UUO at day 1 and continued to be expressed during the development of renal fibrosis. (D) cATF6 protein was induced by UUO. (E) Both phosphorylated and total inositol-requiring 1 (IRE1 α) were enhanced after 3 d of UUO, and more significant induction of these proteins occurred at days 7 and 14 of UUO. (F) Splicing (s) and unsplicing (u) XBP-1 were both attenuated after 1 d of UUO. After 14 d of UUO, only 20% of sXBP-1 and 8% of uXBP-1 were maintained. Data are presented as mean \pm standard error of the mean (SEM) ($n = 3-5$ per group). * $P < 0.05$ versus control group.

phosphorylation induction, which were associated with the lower cleavage of PARP and caspase-12 at d 14 after UUO

(see Figure 6). With administration of CAN, GRP78 induction was also maintained for all 14 d in the UUO kidney. Of

interest, CAN treatment also restored XBP-1 protein and was associated with diminished caspase-12 and JNK phosphorylation. CAN treatment diminished the overwhelming ER stress signals, which was consistent with the lower levels of renal apoptosis, as shown by lower PARP cleavage (see Figure 6B) and TUNEL-positive cells (Figure 7), and renal fibrosis as shown by lesser α -smooth muscle actin (α -SMA) expression (see Figure 6B) and Masson Trichrome staining (Figure 8).

DISCUSSION

This study demonstrated that activation of ER stress is critical for tubular cell loss and renal fibrosis in the UUO fibrosis model. Adding CAN modified ER stress signals and significantly attenuated tubular cell apoptosis and renal fibrosis. These data connect a possible causative role for ER stress with the development of progressive kidney fibrosis. They also argue for ER stress-related targets as potential therapeutic targets.

The ER-luminal domain of PERK, IRE1 α and ATF6 proteins interacts with the ER retention protein GRP78 in the resting state. In response to different cellular stresses, these molecules dissociate from GRP78 and activate the signaling cascades of adaptive UPRs and, if stress persists, subsequent overwhelming ER stress (8). To discover what activates ER stress in rat kidneys after UUO, we assessed the expression of GRP78 and other ER retention proteins with KDEL sequences. As shown in Figure 3A, GRP78 protein was increased in the kidneys of rats treated with UUO within 1 day and lasted, albeit slightly attenuated, until renal fibrosis developed at day 14. In addition to GRP78, both GRP94 and protein disulfide isomerase share the carboxy-terminal KDEL sequence. These retention proteins appear to be necessary to maintain protein-folding capacity in the ER. The expression of KDEL supported the induction of adaptive UPRs in UUO kidney (see Figures 3B–D). It is well known that the induction of UPR allows cells to recover from stress. In contrast, substan-

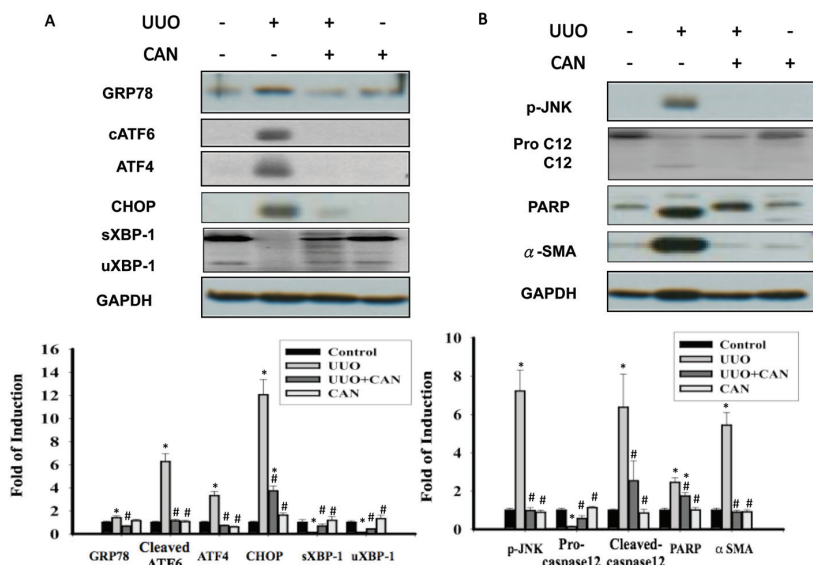


Figure 6. CAN reversed the activation of overwhelming ER stress signaling pathways. (A) Protein levels of GRP78, cATF6 (50 kDa), ATF4, CHOP and unsplicing and splicing XBP-1 (uXBP-1 and sXBP-1). cATF6, ATF4 and CHOP were suppressed by CAN in the UO kidney. sXBP-1 and uXBP-1 proteins were restored by CAN in the UO kidney. (B) Protein levels of the phosphorylated JNK, procaspase-12, PARP and α -SMA. Caspase 12, phosphorylated JNK and PARP were attenuated by CAN at day 14 in the UO kidney. CAN also suppressed α -SMA, which suggests less renal fibrosis and epithelial-mesenchymal transition in CAN-treated kidney. Data are presented as mean \pm standard error of the mean (SEM) (n = 3–5 per group). **P* < 0.05 versus control group; #*P* < 0.05 versus UO group.

tial or prolonged ER stress may be cytotoxic and lead to apoptosis. To confirm that GRP78 activation was associated with upregulation of ER stress-related signals, we assessed the expression of cATF6, ATF4 and IRE1 α . It has been known that ER-stress-induced apoptosis is mainly mediated by CHOP, which is downstream of the PERK (PERK-eIF2 α -ATF4 pathway) and cATF6 pathway. Furthermore, IRE1 α activates both the caspase-12-dependent and JNK-mediated apoptotic pathways. In our observation, cATF6 protein, in parallel with the induction of proapoptotic transcriptional factor CHOP, was observed on day 1 after UO. The phenomenon lasted and was enhanced until renal fibrosis developed at day 14 (see Figures 5A–D). ER-associated apoptotic signals, including caspase-12 and CHOP, were also activated after UO (see Figures 4B, D). These findings confirmed the activation of UPRs and subsequent overwhelming ER stress in the progressive kidney fibrosis models. However, phosphorylation of JNK was observed 1 day after UO operation, but

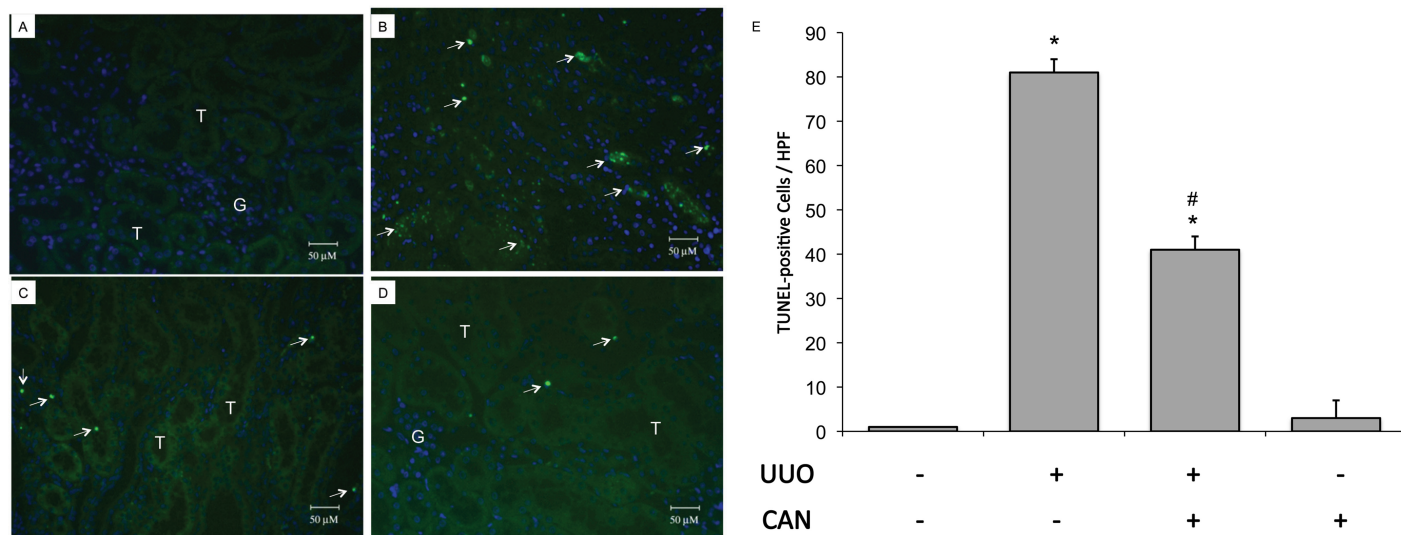


Figure 7. CAN attenuated renal cell apoptosis in rat UO kidney. Apoptosis was evaluated via a TUNEL assay. (A) Sham-operative kidneys show no positive nuclear stain for TUNEL. (B) UO kidney showed a significant increase in TUNEL-positive staining at day 14. (C) CAN significantly attenuated UO-induced renal cells apoptosis, as shown by TUNEL-positive staining at day 14. (D) CAN-treated sham-operative kidneys showed no significant difference compared with the sham-operative group in TUNEL staining. (E) The TUNEL-positive staining cells of the kidney tissue calculated as described in Materials and Methods were averaged for rats of each group (n = 3 for each group). G indicates glomerulus and T is renal tubule. **P* < 0.05 versus the sham operation (Sham) group. #*P* < 0.05 versus the UO group. The arrows indicate TUNEL-positive cells. 4',6-Diamidino-2-phenylindole (DAPI) staining was used to stain the nuclei blue. HPF, high power field.

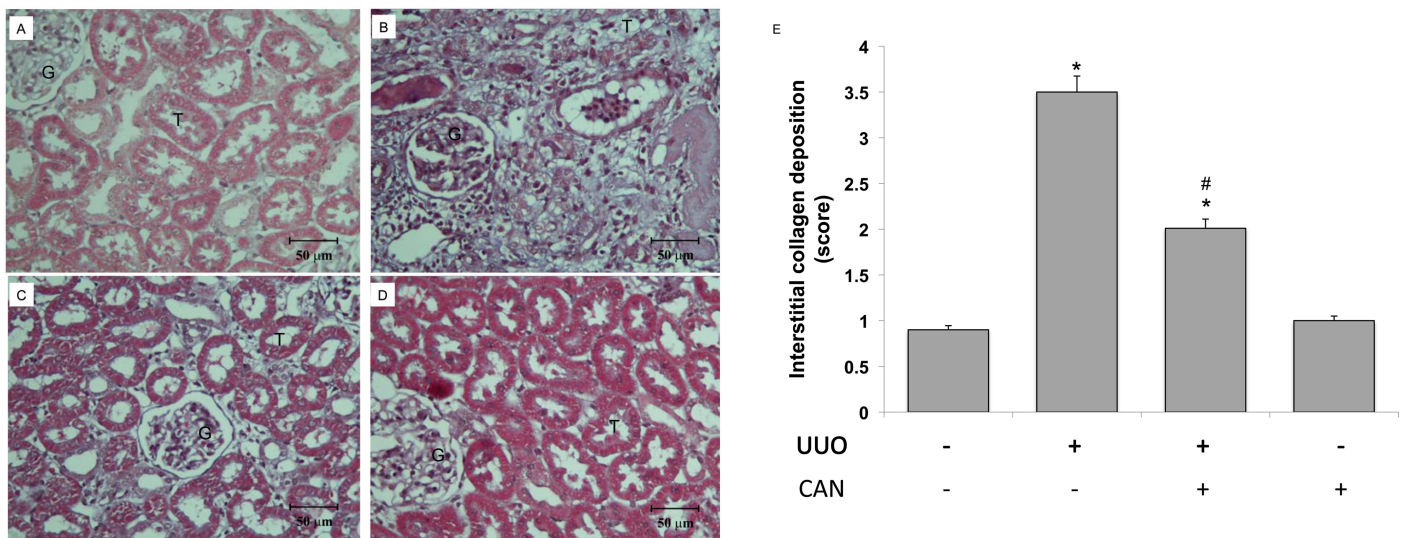


Figure 8. CAN attenuated collagen deposition in rat UUO kidney. The left kidneys of male Wistar rats were subjected to UUO as described in Materials and Methods. Oral gavage with CAN (2.5 mg/kg, twice a day) was delivered from day 1 to day 14 of UUO. At 14 d after UUO, the kidneys were harvested and cut into 6- μ m-thick slices for Masson trichrome staining. (A) Sham-operative kidneys showed no positive Masson trichrome staining. Progressive tubular dilation, interstitial volume expansion and development of fibrosis were observed after 14 d of UUO (B), and CAN significantly attenuated UUO-induced interstitial damages and fibrosis (C). (D) CAN-treated sham operative did not show the interstitial damages and fibrosis. (E) The degree of interstitial collagen deposits in Masson trichrome-stained sections of the kidney tissue graded semiquantitatively as described in Materials and Methods were averaged for rats of each group ($n = 3$ for each group). G indicates glomerulus and T is renal tubule. * $P < 0.05$ versus the sham operation (Sham) group. # $P < 0.05$ versus the UUO group.

phosphorylation of IRE1 α was upregulated 3 days after UUO. ER stress may contribute to the late, but not the early, phase of JNK phosphorylation.

Upon ER stress, a 26-bp intron of the XBP-1 pre-mRNA is spliced out by increased IRE1 α endoribonuclease activity, resulting in synthesis of the potent XBP-1 transcription factor (8). The target genes of XBP-1 enhance the folding capacity and degradation efficiency of ER proteins, in turn increasing its cytoprotective function (33). Recent data have shown that XBP-1 mRNA splicing levels decline after prolonged ER stress, whereas PERK signaling is sustained over time (34). Inactivation of XBP-1 splicing may sensitize cells to cell death after chronic or irreversible ER stress. Similarly, knocking down XBP-1 enhances cell death under conditions of chronic ER stress (35). We demonstrated that both splicing and unsplicing XBP-1 protein expressions were attenuated as tubular dilation and renal fibrosis progressed in the UUO kidney (see Figure 5F). Therefore, selectively lowering the adaptive UPR signals, such

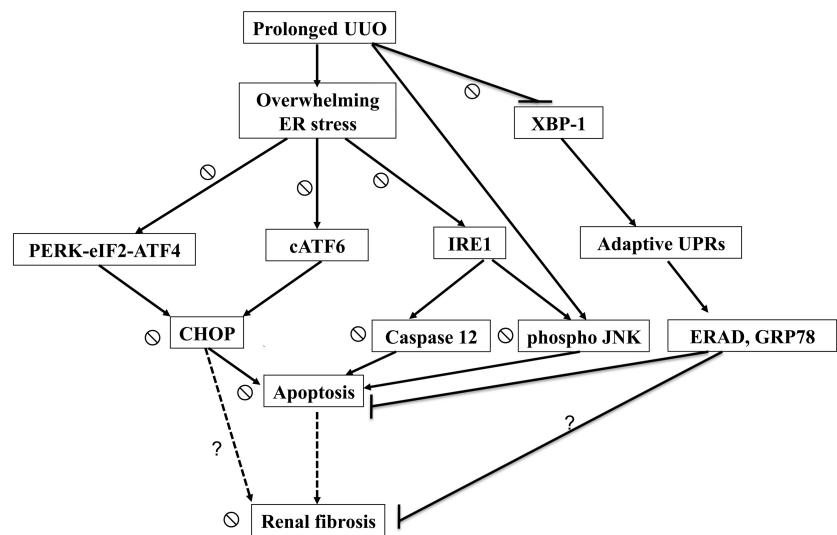


Figure 9. Schematic representation of proposed mechanisms that ER stress leading to the renal cells apoptosis and fibrosis in the UUO kidneys. Prolonged UUO activated overwhelming ER stress, including PERK-eIF2 α -ATF4-CHOP, ATF6-CHOP and IRE1 α -JNK/IRE1 α -caspase-12 signals, leading to renal cells apoptosis. In contrast, UUO attenuated XBP-1-related adapted UPRs, which associated with antiapoptotic properties of ER-associated degradation and GRP78. Loss of renal cells is associated with inadequate tubular interstitial integrity and renal fibrosis. CAN attenuated overwhelming ER stress-related signals and restored adaptive XBP-1 activity. The dashed arrow represents the ratiocination of renal fibrosis. The \odot symbol indicates the action of CAN on ER stress-related signals in the UUO kidney. The question mark indicates the potential ER stress-related pathways leading to renal fibrosis in the UUO kidney.

as XBP-1 expression, may lower cellular protection. On the other hand, the downstreams signals of IRE1 α , such as activation of caspase-12 and JNK, help initiate ER stress-mediated apoptosis (8,18,35). In this work, caspase-12 activation was observed in UUO kidneys at days 3, 7 and 14 (see Figure 4B). This result implied that apoptosis was induced in UUO kidneys, at least in part, through BAX activation and IRE1 α phosphorylation (see Figures 4A and 5E). This hypothesis was supported by previous observations that caspase-12 cleavage and activation is one of the hallmarks of ER-mediated cell death by cytotoxins in renal tubular cells (36,37). We suppose that selective activation of IRE1 α downstream proapoptotic and antiapoptotic signaling leads to completely different fates for renal cells. Actually, ER stress was proven to induce epithelial-to-mesenchymal transformation in human proximal tubule cells, a finding that directly connects ER stress to renal fibrosis (22,27,38). Furthermore, the accumulation of uremic toxins may further contribute to the deterioration of renal function in advanced chronic kidney disease. Recently, Kawakami *et al.* (39) showed that a representative uremic toxin, indoxyl sulfate, suppressed the proliferation of human proximal tubular cells by ER stress-dependent pathways. Our results strongly suggest that ER stress pathways are potential targets for retarding chronic kidney disease progression.

Furthermore, we demonstrated that CAN modulates a differential activation of the ER chaperones, suppressing the development of renal cell apoptosis and fibrosis in UUO kidneys. CAN maintains the expression of XBP-1 protein, which was functionally linked to enhancement of the adaptive survival signals under ER stress in UUO kidney (see Figure 6). In an adult cardiac myocyte model, CAN prevented angiotensin II increases in ER chaperones as well as protein synthesis. These findings suggest that an angiotensin II type 1 receptor-dependent pathway contributes to the activation of ER stress

and cell apoptosis (19). Recent reports also suggest that angiotensin-converting enzyme inhibitor suppresses the apoptosis induced by ER stress in renal tubules of experimental diabetic rats (40). Some may object to the numerous mechanisms of the renin-angiotensin system blockade involved in cell protection, including reversing hypoxia, ischemia and hypertension and suppressing reactive oxygen species; however, cellular stress mechanisms frequently operate through complex networks. Therapeutic approaches with ARB may act to break the vicious cycle of oxidative stress, hypoxia and ER stress (8). Because the detailed mechanisms by which the angiotensin system contributes to the induction of ER stress are still unknown, further investigation of the intracellular signaling pathway by which angiotensin II induces ER stress in renal cells is warranted.

To prove the direct evidence that ER stress contributed to the development of renal fibrosis, we arranged 4-phenylbutyrate (4-PBA, an ER chemical chaperon) treatments in a UUO rat model (41). 4-PBA successfully attenuated ER stress and suppressed the expression of collagen type 1 α , fibronectin and α -SMA in UUO kidneys (Supplementary Figure 1). We also introduced UUO in *chop* deficiency mice and found *chop* knockout successfully attenuated the development of renal fibrosis (unpublished data). These preliminary results supported that attenuated ER stress by chemical chaperon or block ER-related proapoptotic signals by CHOP deletion suppressed renal fibrosis. Further investigations to explore the mechanisms of how ER stress modulated the renal fibrosis are mandatory.

In conclusion, this study demonstrated that the activation of overwhelming ER stress is associated with UUO-induced renal apoptosis and fibrosis in a rat model. As indicated in Figure 9, activation of overwhelming ER stress and attenuation of adaptive UPRs triggered renal apoptosis and consequent fibrosis in UUO kidney. CAN successfully reversed these signals and attenuated

renal fibrosis. It is warranted to study the potential benefits of modulating adaptive UPRs in chronic kidney disease treatment.

ACKNOWLEDGMENTS

We thank the Second Core Laboratory of the Department of Medical Research in the National Taiwan University Hospital for equipment and facility support. This work was supported by grants from the National Science Council (to C-K Chiang: NSC-97-2314-B-002-051 and NSC-100-2314-B-002-069) and the Taiwan University Hospital (to C-K Chiang: NTUH-99-S-1333 and 98-FTN01).

DISCLOSURE

The authors declare that they have no competing interests as defined by *Molecular Medicine*, or other interests that might be perceived to influence the results and discussion reported in this paper.

REFERENCES

- Hewitson TD. (2009) Renal tubulointerstitial fibrosis: common but never simple. *Am. J. Physiol. Renal Physiol.* 296:F1239-44.
- Risdon RA, Sloper JC, De Wardener HE. (1968) Relationship between renal function and histological changes found in renal-biopsy specimens from patients with persistent glomerular nephritis. *Lancet.* 2:363-6.
- Liu Y. (2006) Renal fibrosis: new insights into the pathogenesis and therapeutics. *Kidney Int.* 69:213-7.
- Mimura I, Nangaku M. (2010) The suffocating kidney: tubulointerstitial hypoxia in end-stage renal disease. *Nat. Rev. Nephrol.* 6:667-78.
- Nangaku M. (2006) Chronic hypoxia and tubulointerstitial injury: a final common pathway to end-stage renal failure. *J. Am. Soc. Nephrol.* 17:17-25.
- Docherty NG, O'Sullivan OE, Healy DA, Fitzpatrick JM, Watson RW. (2006) Evidence that inhibition of tubular cell apoptosis protects against renal damage and development of fibrosis following ureteric obstruction. *Am. J. Physiol. Renal Physiol.* 290:F4-13.
- Klahr S, Morrisey J. (2002) Obstructive nephropathy and renal fibrosis. *Am. J. Physiol. Renal Physiol.* 283:F861-75.
- Inagi R. (2010) Endoplasmic reticulum stress as a progression factor for kidney injury. *Curr. Opin. Pharmacol.* 10:156-65.
- Malhotra JD, Kaufman RJ. (2007) Endoplasmic reticulum stress and oxidative stress: a vicious cycle or a double-edged sword? *Antioxid. Redox Signal.* 9:2277-93.

10. Yoshida H. (2007) ER stress and diseases. *FEBS J* 274:630–58.
11. Inagi R, *et al.* (2005) Involvement of endoplasmic reticulum (ER) stress in podocyte injury induced by excessive protein accumulation. *Kidney Int.* 68:2639–50.
12. Hotamisligil GS. (2010) Endoplasmic reticulum stress and the inflammatory basis of metabolic disease. *Cell.* 140:900–17.
13. Hong M, Li M, Mao C, Lee AS. (2004) Endoplasmic reticulum stress triggers an acute proteasome-dependent degradation of ATF6. *J. Cell. Biochem.* 92:723–32.
14. Shen J, Prywes R. (2004) Dependence of site-2 protease cleavage of ATF6 on prior site-1 protease digestion is determined by the size of the luminal domain of ATF6. *J. Biol. Chem.* 279:43046–51.
15. Oyadomari S, Araki E, Mori M. (2002) Endoplasmic reticulum stress-mediated apoptosis in pancreatic beta-cells. *Apoptosis.* 7:335–45.
16. Han D, *et al.* (2009) IRE1 α kinase activation modes control alternate endoribonuclease outputs to determine divergent cell fates. *Cell.* 138:562–75.
17. Korennykh AV, *et al.* (2009) The unfolded protein response signals through high-order assembly of Ire1. *Nature.* 457:687–93.
18. Cybulsky AV. (2010) Endoplasmic reticulum stress in proteinuric kidney disease. *Kidney Int.* 77:187–93.
19. Okada K, *et al.* (2004) Prolonged endoplasmic reticulum stress in hypertrophic and failing heart after aortic constriction: possible contribution of endoplasmic reticulum stress to cardiac myocyte apoptosis. *Circulation.* 110:705–12.
20. Mu YP, Ogawa T, Kawada N. (2010) Reversibility of fibrosis, inflammation, and endoplasmic reticulum stress in the liver of rats fed a methionine-choline-deficient diet. *Lab. Invest.* 90:245–56.
21. Tamaki N, *et al.* (2008) CHOP deficiency attenuates cholestasis-induced liver fibrosis by reduction of hepatocyte injury. *Am. J. Physiol. Gastrointest. Liver Physiol.* 294:G498–505.
22. Dickhout JG, Carlisle RE, Austin RC. (2011) Interrelationship between cardiac hypertrophy, heart failure, and chronic kidney disease endoplasmic reticulum stress as a mediator of pathogenesis. *Circ. Res.* 108:629–42.
23. Dihazi H, *et al.* (2011) Proteomics characterization of cell model with renal fibrosis phenotype: osmotic stress as fibrosis triggering factor. *J. Proteomics.* 74:304–18.
24. Higgins DF, *et al.* (2007) Hypoxia promotes fibrogenesis in vivo via HIF-1 stimulation of epithelial-to-mesenchymal transition. *J. Clin. Invest.* 117:3810–20.
25. el-Dahr SS, *et al.* (1993) Upregulation of renin-angiotensin system and downregulation of kallikrein in obstructive nephropathy. *Am. J. Physiol.* 264:F874–81.
26. Badiola N, *et al.* (2011) Induction of ER stress in response to oxygen-glucose deprivation of cortical cultures involves the activation of the PERK and IRE-1 pathways and of caspase-12. *Cell Death Dis.* 2:e149.
27. Lee JY, *et al.* (2011) Albumin-induced epithelial-mesenchymal transition and ER stress are regulated through a common ROS-c-Src kinase-mTOR pathway: effect of imatinib mesylate. *Am. J. Physiol. Renal Physiol.* 300:F1214–22.
28. Yeh CH, Chiang HS, Lai TY, Chien CT. (2011) Unilateral ureteral obstruction evokes renal tubular apoptosis via the enhanced oxidative stress and endoplasmic reticulum stress in the rat. *Neurorol. Urodyn.* 30:472–9.
29. Moriyama T, *et al.* (1997) TCV-116 inhibits interstitial fibrosis and HSP47 mRNA in rat obstructive nephropathy. *Kidney Int. Suppl.* 63:S232–5.
30. Yu C, Gong R, Rifai A, Tolbert EM, Dworkin LD. (2007) Long-term, high-dosage candesartan suppresses inflammation and injury in chronic kidney disease: nonhemodynamic renal protection. *J. Am. Soc. Nephrol.* 18:750–9.
31. Remuzzi G, *et al.* (1999) Combining an antiproteinuric approach with mycophenolate mofetil fully suppresses progressive nephropathy of experimental animals. *J. Am. Soc. Nephrol.* 10:1542–9.
32. Munro S, Pelham HR. (1987) A C-terminal signal prevents secretion of luminal ER proteins. *Cell.* 48:899–907.
33. Ron D, Walter P. (2007) Signal integration in the endoplasmic reticulum unfolded protein response. *Nat. Rev. Mol. Cell. Biol.* 8:519–29.
34. Lin JH, *et al.* (2007) IRE1 signaling affects cell fate during the unfolded protein response. *Science.* 318:944–9.
35. Lisbona F, *et al.* (2009) BAX inhibitor-1 is a negative regulator of the ER stress sensor IRE1 α . *Mol. Cell.* 33:679–91.
36. Muruganandan S, Cribb AE. (2006) Calpain-induced endoplasmic reticulum stress and cell death following cytotoxic damage to renal cells. *Toxicol. Sci.* 94:118–28.
37. Ryan PM, Bedard K, Breining T, Cribb AE. (2005) Disruption of the endoplasmic reticulum by cytotoxins in LLC-PK1 cells. *Toxicol. Lett.* 159:154–63.
38. Pallet N, *et al.* (2008) Cyclosporine-induced endoplasmic reticulum stress triggers tubular phenotypic changes and death. *Am. J. Transplant.* 8:2283–96.
39. Kawakami T, Inagi R, Wada T, Tanaka T, Fujita T, Nangaku M. (2010) Indoxyl sulfate inhibits proliferation of human proximal tubular cells via endoplasmic reticulum stress. *Am. J. Physiol. Renal Physiol.* 299:F568–76.
40. Sun HL, *et al.* (2009) ACE-inhibitor suppresses the apoptosis induced by endoplasmic reticulum stress in renal tubular in experimental diabetic rats. *Exp. Clin. Endocrinol. Diabetes.* 117:336–44.
41. Qi W, *et al.* (2011) Attenuation of diabetic nephropathy in diabetes rats induced by streptozotocin by regulating the endoplasmic reticulum stress inflammatory response. *Metabolism.* 60:594–603.